1798 *Chem. Mater.* **2010,** *22,* 1798–1806
DOI:10.1021/cm903300y

CHEMISTRY OF MATERIALS
Article

$EuAg_xAl_{11-x}$ with the $BaHg_{11}$-Type Structure: Composition, Coloring, and Competition with the $BaCd_{11}$-Type Structure

Fei Wang,[†] Karen N. Pearson,[‡] Warren E. Straszheim,[§] and Gordon J. Miller*,[†]

[†]*Department of Chemistry, Iowa State University, Ames, Iowa 50011,* [‡]*Department of Chemistry, Hope College, Holland, MI 49422, and* [§]*Materials Analysis and Research Lab, Iowa State University, Ames, Iowa 50011*

Received October 28, 2009. Revised Manuscript Received December 2, 2009

$EuAg_xAl_{11-x}$ phases adopting the $BaHg_{11}$-type structure (space group $Pm\bar{3}m$, $Z = 3$) were synthesized with high yield by arc melting a mixture loaded as "$EuAg_{3.5}Al_{7.5}$" and annealing at 500 °C for 40 days. This phase has a very narrow phase width around $EuAg_{4.0}Al_{7.0}$; and it is unstable at 600 and 700 °C, at which it transforms into other phases. Magnetometry indicates that Eu is divalent, which gives the valence electron concentration per Ag/Al atom as 2.45 e^-/atom, higher than in the $BaCd_{11}$-type phases in the Eu−Ag−Al system (2.10−2.30 e^-/atom). First principles electronic structure calculations, using a computational model structure built by simulating the crystallographic results as well as maximizing the number of heteroatomic (Ag−Al) contacts, can explain why the cubic $BaHg_{11}$-type structure is favored at higher valence electron concentration than the tetragonal $BaCd_{11}$-type structure.

Introduction

Polar intermetallics[1−3] represent a growing class of compounds bridging classical, Hume−Rothery electron phases[4] and Zintl phases.[5] Similar to Zintl phases, polar intermetallics also consist of elements with considerable differences in electronegativity, but their structures cannot be understood with the octet rule, which applies to Zintl phases; instead, as in Hume−Rothery phases, they are largely determined by valence electron count. However, unlike Hume−Rothery electron phases, polar intermetallics often form kaleidoscopic complex structures, for example, $NaZn_{13}$-, $ThMn_{12}$-, $BaCd_{11}$-, and $BaHg_{11}$-types, in which, just as in Zintl phases, the "cations", that is, the electropositive metals, have large coordination numbers. Many recent reports also showed that this class of compounds provides a wealth of quasicrystalline phases and their crystalline approximants.[6] Because of such structural abundance and complexity, composition-structure relationships of polar intermetallic compounds are complicated and still remain a challenge to be understood. Further systematic investigations into polar intermetallics are necessary; and these investigations will benefit from a synergism between experiment and theory.

During our investigations into the composition-structure relationship in polar intermetallics, significant effort has been devoted to the RE(rare earth)−Ag−Al systems due to their structural abundance.[7] Researchers have obtained kaleidoscopic complex structures from these systems, including the $BaCd_{11}$-, $BaHg_{11}$-, Th_2Ni_{17}-, Th_2Zn_{17}-, $CaCu_5$-, and $BaAl_4$-types.[8] The iso-compositional structure types (i.e., the $BaCd_{11}$- vs $BaHg_{11}$-types and the Th_2Ni_{17}- vs Th_2Zn_{17}-types) often compete within a single RE−Ag−Al system as its composition varies. For instance, in Yb−Ag−Al, the $BaCd_{11}$-type structure forms at $YbAg_{5.3}Al_{5.7}$ and the $BaHg_{11}$-type structure forms at $YbAg_4Al_7$.[8l] Similar results have also been obtained in our previous work with the Eu−Ag−Al system.[9] Further investigations into these competing structure types can deepen our understanding of

*Author to whom correspondence should be addressed. E-mail: gmiller@iastate.edu.

(1) (a) Belin, C.; Tillard-Charbonnel, M. *Prog. Solid State Chem.* **1993**, *22*, 59. (b) Belin, C.; Tillard-Charbonnel, M. *Coord. Chem. Rev.* **1998**, *180*, 529.
(2) Corbett, J. D. *Angew. Chem., Int. Ed.* **2000**, *39*, 670.
(3) Häussermann, U.; Amerioun, S.; Eriksson, L.; Lee, C.-S.; Miller, G. J. *J. Am. Chem. Soc.* **2002**, *124*, 4371.
(4) Hume-Rothery, W.; Raynor, G. V. *The Structure of Metals and Alloys*, 1st ed; The Institute of Metals: London, 1936.
(5) Schäfer, H.; Eisenmann, B.; Müller, W. *Angew. Chem., Int. Ed.* **1973**, *12*(9), 694.
(6) (a) Lin, Q.; Corbett, J. D. *J. Am. Chem. Soc.* **2005**, *127*, 12786. (b) Lin, Q.; Corbett, J. D. *J. Am. Chem. Soc.* **2007**, *129*, 6789.
(7) Nordell, K. J. Exploring Aluminum-Rich Intermetallics with Experiment and Theory. Ph.D. Thesis, Iowa State University, Ames, IA, **1997**.
(8) (a) Denysyuk, O. V.; Stel'makhovych, B. M.; Kuz'ma, Yu. B. *J. Solid State Chem.* **1994**, *109*, 172. (b) Stel'makhovych, B. M.; Kuz'ma, Yu. B. *Dopov. Nats. Akad. Nauk Ukr.* **1994**, *3*, 86. (c) Zhak, O. V.; Stel'makhovych, B. M.; Kuz'ma, Yu. B. *Russ. Metall.* **1995**, *6*, 158. (d) Kuz'ma, Yu. B.; Zhak, O. V.; Shkolyk, S. Yu. *Dopov. Nats. Akad. Nauk Ukr.* **1995**, *3*, 101. (e) Zhak, O. V.; Stel'makhovych, B. M.; Kuz'ma, Yu. B. *J. Alloys Comp.* **1996**, *237*, 144. (f) Kuz'ma, Yu. B.; Zhak, O. V.; Sarapina, O. S. *Russ. Metall.* **1997**, *2*, 166. (g) Zhak, O. V.; Kuz'ma, Yu. B. *J. Alloys Comp.* **1999**, *291*, 175. (h) Stel'makhovych, B. M.; Gumenyuk, T. M.; Kuz'ma, Yu. B. *J. Alloys Comp.* **2000**, *298*, 164. (i) Gumeniuk, R. V.; Stel'makhovych, B. M.; Kuz'ma, Yu. B. *J. Alloys Comp.* **2001**, *321*, 132. (j) Stel'makhovych, B. M.; Zhak, O. V.; Bilas, N. R.; Kuz'ma, Yu. B. *J. Alloys Comp.* **2004**, *363*, 243. (k) Cordier, G.; Dörsam, G.; Kniep, R. *J. Magn. Magn. Mater.* **1988**, *76 & 77*, 653. (l) Schank, C.; Tegel, U.; Henseleit, R.; Grauel, A.; Olesch, G.; Geibel, C.; Cordier, G.; Kniep, R.; Steglich, F. *J. Alloys Comp.* **1994**, *207*/*208*, 333.
(9) Wang, F.; Pearson, K. N.; Miller, G. J. *Chem. Mater.* **2009**, *21*, 230.

Published on Web 01/07/2010

these structures themselves, as well as how they are related to composition.

The $BaHg_{11}$-type structure is one of the most rarely observed among all of the complex structures obtained in RE−Ag−Al ternaries. It has been reported only with RE = Ce,[8k] Yb,[8l], and Eu[9] without crystallographic details (only lattice parameters available, without atomic coordinates or thermal parameters). Experimental disagreement also occurs in the Ce−Ag−Al system. Although Cordier obtained $BaHg_{11}$-type $CeAg_{3.1}Al_{7.9}$ by synthesizing at 1000−1400 °C and annealing at 800 °C,[8k] this phase did not occur in Kuz'ma's phase diagram study at 597 °C,[8c] which was proposed as a temperature effect. The recent reports from Latturner et al. demonstrated more complexity of the $BaHg_{11}$-type structure.[10] Their study of RE−Au−Al and RE−Ag−Al systems showed that, in an Al flux, early transition metals (e.g., Ti and Mo) have a template effect and are essential in the formation of a stuffed $BaHg_{11}$-type structure, which is a quaternary phase, $RE_3(Au/Ag)_{6+x}Al_{26}T$ (T is the early transition metal). The authors also analyzed the synthesis method adopted by Cordier[8k,l] and speculated that the possible inclusion of Mo (the crucible material) induced the formation of the $BaHg_{11}$-type structure.

Therefore, although the $BaHg_{11}$-type structure has been long observed in RE−Ag−Al systems, there are still many unsolved "mysteries" about it, for example, what the phase width is, and how temperature and early transition metals affect its formation. Moreover, site sharing and site preference are commonly observed for Ag and Al atoms in RE−Ag−Al systems. How are Ag and Al distributed in the $BaHg_{11}$-type structure? Lastly, how does this structure type compete with the $BaCd_{11}$-type structure during changes in composition, viz., the molar ratio between Ag and Al, of a RE−Ag−Al system? To answer these questions, we continued our previous work with the $EuAg_xAl_{11-x}$ system[9] and investigated $BaHg_{11}$-type phases using both experiments and quantum mechanical calculations.

Experimental Section

Syntheses. Pure metals were used for syntheses: Eu (rods, Ames Laboratory, 99.99%), Ag (slugs, Alfa Aesar, 99.99%), and Al (foil, Tenneco). In our previous study of $EuAg_xAl_{11-x}$, the $BaHg_{11}$-type structure was observed in the systems loaded with "$EuAg_4Al_7$" and "$EuAg_3Al_8$".[9] To find out its homogeneity width, we varied the loading composition from "$EuAg_4Al_7$" to "$EuAgAl_{10}$". For each loading composition, an approximately 0.5 g mixture of pure metals was arc melted under an argon atmosphere into a silvery button, which was turned over and remelted five times to ensure thorough reaction and homogeneity. There was some ash generated during melting, but the weight loss was always lower than 1 wt %. Every product was stable in air and water but dissolved in 40 wt % nitric acid. The silvery button was then broken into halves. One-half was characterized immediately; and the other half, before characterization, was sealed in a tantalum tube under argon atmosphere, which was then sealed in an evacuated silica jacket and annealed in a tube furnace at 500 °C for 40 days.

X-ray Crystallography. Powder X-ray diffraction (XRD) was carried out on a Huber Imaging Plate Guinier Camera G670 using monochromatized Cu $K\alpha_1$ radiation (λ = 1.54059 Å). This diffractometer has been calibrated with standard silicon powder (NIST, a = 5.430940 ± 0.000035 Å). The exposure time was 1 h and the step size of 2θ was 0.005°. The Le Bail technique[11] was used for full pattern decomposition, and the Rietveld method[12] was employed to refine the crystal structure, both of which were accomplished with the software *LHPM-Rietica*.[13]

Small crystals selected from the crushed "$EuAg_{3.5}Al_{7.5}$" sample were mounted on the tip of capillary with epoxy for single-crystal XRD experiments, which were carried out at room temperature on a STOE IPDS diffractometer equipped with Mo Kα radiation (λ = 0.71073 Å). 80 frames were collected at φ = 130° with ω ranging from 42 to 122° with the step size of 1°, and the exposure time of 1 min per frame. All data collection, integrations, cell refinements, and absorption corrections were done using *X-Area*.[14] Using *SHELXTL*,[15] the crystal structure was solved with direct methods and refined by full-matrix least-squares on F^2.

Magnetometry. Temperature-dependent magnetic susceptibility was measured with a 6.3 mg sample taken from the annealed product with the loading composition "$EuAg_{3.5}Al_{7.5}$", which is a "pure phase" adopting the $BaHg_{11}$-type structure according to powder XRD. Using a Quantum Design MPMS XL Superconducting Quantum Interference Device (SQUID) magnetometer, at 1 kOe fixed magnetic field, the magnetic susceptibility (χ) was measured as the temperature (T) varied from 5 to 300 K. We fitted the $1/\chi$ vs T curve with Curie−Weiss law to calculate the effective moment (μ_{eff}) and the valency of Eu.

Microscopy. The annealed sample loaded as "$EuAg_{3.5}Al_{7.5}$" was also characterized by scanning electron microscopy (SEM) and energy-dispersive spectroscopy (EDS) to examine its homogeneity and to check the presence of early transition metals, including W (electrode material of the arc melter), Ti (oxygen getter), and Ta (container for annealing). SEM was accomplished using a Hitachi S-2460N variable-pressure scanning electron microscope, and EDS was performed with an Oxford Instruments Isis X-ray analyzer. Several grains were taken at random from the broken "$EuAg_{3.5}Al_{7.5}$" sample, embedded in epoxy, polished, coated with ca. 20 nm of carbon, and examined in high vacuum mode (ca. 5×10^{-6} Torr). The accelerating voltage was 20 kV and the beam current was ca. 0.5 nA, which produced an X-ray count rate of 3000 cps. Multiple points were examined for every sample grain. The standards used for quantitative compositional analysis were elemental Ag and Al, and $EuAl_2$. The precision of the compositional analysis under these conditions is within a few tenths of weight percent.

Electronic Structure Calculations. To study the electronic structure of the $BaHg_{11}$-type $EuAg_xAl_{11-x}$, we constructed a few model structures according to the crystallographic results for first principles calculations. Details of these models can be found in the Computational Models section. Both the Stuttgart

(10) (a) Latturner, S. E.; Kanatzidis, M. G. *Inorg. Chem.* **2004**, *43*, 2. (b) Latturner, S. E.; Bilc, D.; Mahanti, S. D.; Kanatzidis, M. G. *Inorg. Chem.* **2009**, *48*, 1346.

(11) Le Bail, A.; Duroy, H.; Fourquet, J. L. *Mater. Res. Bull.* **1988**, *23*, 447.

(12) Rietveld, H. M. *J. Appl. Crystallogr.* **1969**, *2*, 65.

(13) Hunter, B. A.; Howard, C. J. *LHPM-Rietica*, version 1.71: Australian Nuclear Science and Technology Organization: Menai, Australia, 2000.

(14) *X-Area*; Stoe & Cie. GmbH: Darmstadt, Germany.

(15) *SHELXTL*, version 6.10; Bruker AXS Inc.: Madison, WI, 2000.

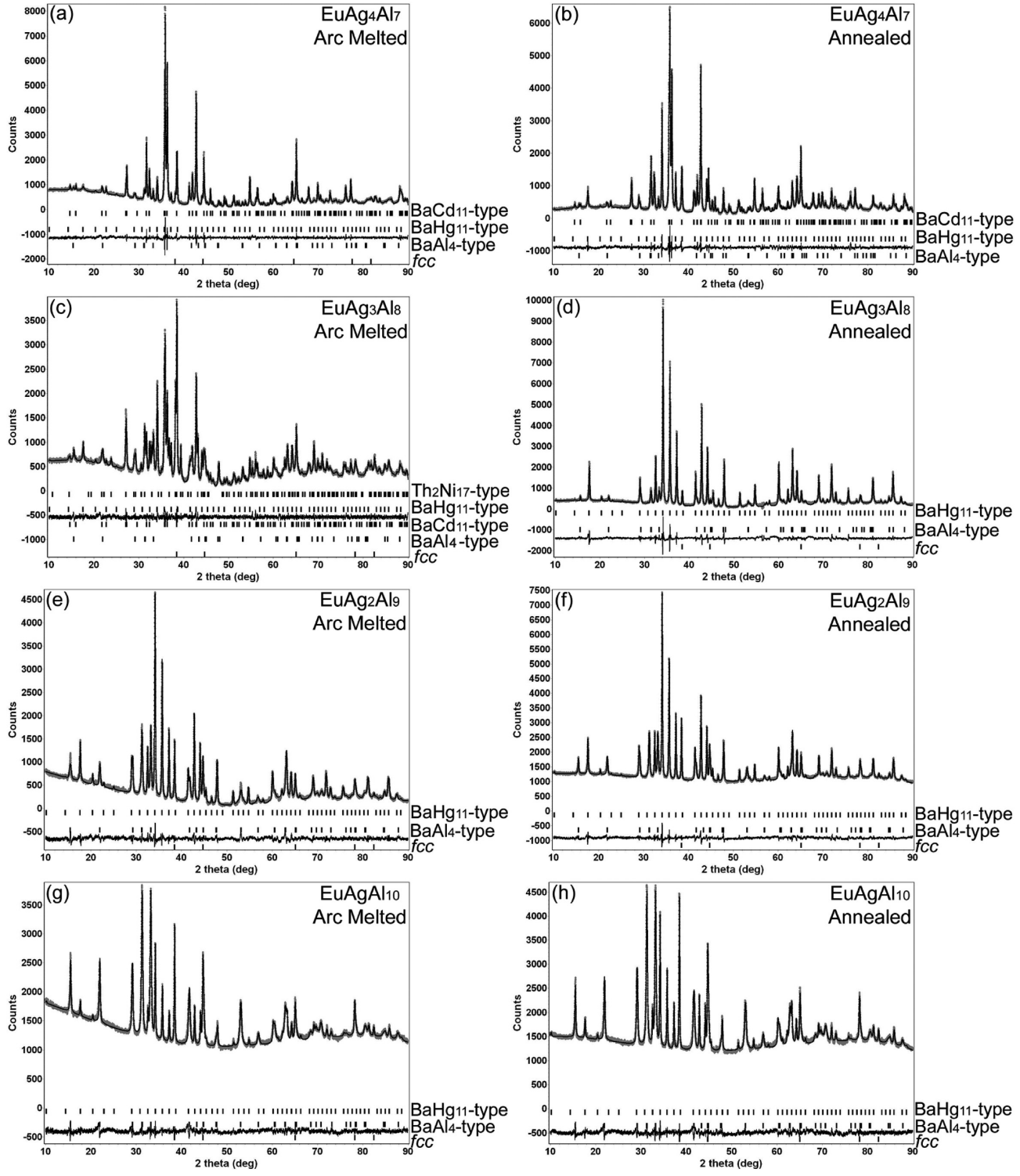

Figure 1. Powder XRD patterns of arc melted and annealed samples with various loading compositions. Le Bail refinement was applied to every pattern.

Tight-Binding, Linear-Muffin-Tin Orbital program with the *Atomic Sphere Approximation* (TB-LMTO-ASA)[16] and the *Vienna ab initio simulation package* (VASP)[17−19] were employed to calculate the total energies and electronic structures of these models.

For TB-LMTO-ASA, we used the von Barth−Hedin local density approximation[20] to treat electron exchange and correlation energy; and we included these atomic orbitals in the basis set: the 6*s*, 6*p* (downfolded[21]), and 5*d* states of Eu; the 5*s*, 5*p*, and 4*d* states of Ag; and the 3*s*, 3*p*, and 3*d* (downfolded) states of Al. Eu 4*f* states were excluded because magnetometry indicated that Eu is divalent and, thus, its 4*f* electrons are localized in half-filled 4*f* orbitals. The Wigner−Seitz radii of the atomic spheres were

(16) Jepsen, O.; Andersen O. K. *TB-LMTO*, version 47; Max-Planck-Institut für Festkörperforschung: Stuttgart, Germany, 2000.
(17) (a) Kresse, G.; Hafner, J. *Phys. Rev. B* **1993**, *47*, 558. (b) Kresse, G.; Hafner, J. *Phys. Rev. B* **1994**, *49*, 14251.
(18) Kresse, G.; Furthmüller, J. *Comput. Mater. Sci.* **1996**, *6*, 15.
(19) Kresse, G.; Furthmüller, J. *Phys. Rev. B* **1996**, *54*, 11169.
(20) von Barth, U.; Hedin, L. *J. Phys. C: Solid State Phys.* **1972**, *5*, 1629.
(21) Lambrecht, W. R. L.; Andersen, O. K. *Phys. Rev. B* **1986**, *34*, 2439.

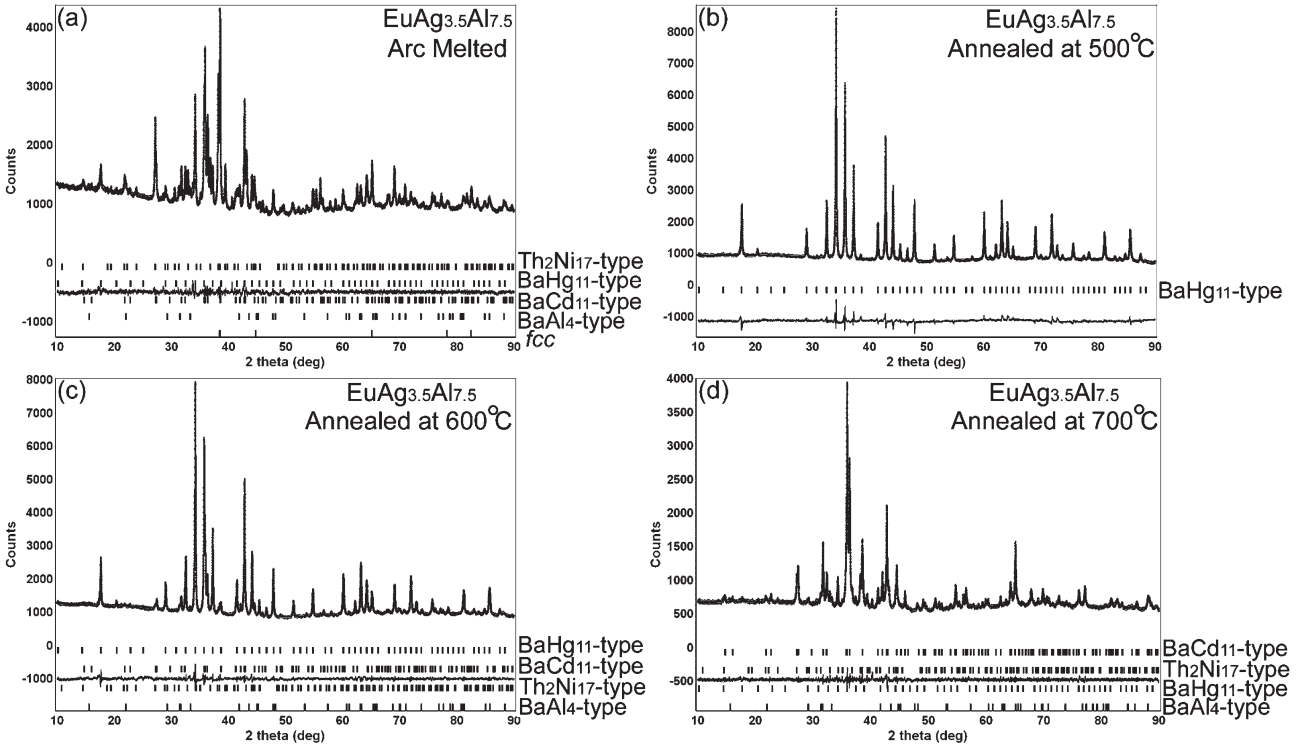

Figure 2. Powder XRD patterns of arc melted and annealed "$EuAg_{3.5}Al_{7.5}$" samples. Le Bail refinement was applied to (a), (c), and (d); and Rietveld refinement was applied to (b).

2.13 Å for Eu and 1.57 Å for both Ag and Al. This filled the unit cell with a 9.566% overlap without introducing any empty spheres; an $8 \times 8 \times 8$ k-points mesh was used in the first Brillouin zone for integration. The density of states (DOS) and crystal orbital Hamiltonian populations (COHP)[22] curves were evaluated and plotted.

VASP calculations were completed to compare the total energies of the model structures. We used the projector augmented-wave (PAW) pseudopotentials[23] and the Perdew−Burke−Ernzerhof generalized gradient approximation (GGA-PBE).[24] The energy cutoff was 343.6 eV. Reciprocal space integrations were completed over a $7 \times 7 \times 7$ Monkhorst-Pack k-points mesh[25] with the linear tetrahedron method.[26] With these settings, the calculated total energy converged to less than 1 meV per atom. The DOS curve calculated by VASP was also plotted and compared with that from TB-LMTO-ASA calculations.

Results and Discussions

Synthesis and X-ray Crystallography. Our previous work[9] indicated that both loading composition and annealing are pertinent to the formation of the $BaHg_{11}$-type structure in $EuAg_xAl_{11-x}$. This cubic structure type was not detected by powder XRD when $x = 5-8$ in the loading composition "$EuAg_xAl_{11-x}$"; but was obtained when $x = 3$ and 4. For both of these two systems, annealing at 500 °C increased the abundance of the $BaHg_{11}$-type phase (see its strongest peak at ca. 34.3° in Figure 1(a)−(d)), especially for the "$EuAg_3Al_8$" system, in which it is the dominant phase.

To improve the abundance of the $BaHg_{11}$-type phase, we adjusted the loading composition. At first, we tested two loading compositions richer in Al than above, viz., "$EuAg_2Al_9$" and "$EuAgAl_{10}$". The diffraction patterns of these arc melted and annealed samples are shown in Figure 1(e)−(h). These two loading compositions produce mixed phases, among which the $BaHg_{11}$-type structure occurs, and annealing at 500 °C also slightly increased its abundance. However, its abundances in these two samples are both lower than in the "$EuAg_3Al_8$" sample (Figure 1(d), (f), (g)).

We then made the Al content lower than in "$EuAg_3Al_8$" and loaded "$EuAg_{3.5}Al_{7.5}$". The powder XRD patterns for arc melted and subsequent annealed samples are in Figure 2. The pattern of the arc melted sample (Figure 2(a)) is close to the arc melted "$EuAg_3Al_8$" system (Figure 1(c)). After annealing at 500 °C, all peaks in the powder pattern can be indexed with a single $BaHg_{11}$-type phase (Figure 2(b)). It is noticeable that the backgrounds in these diffraction patterns are large (ca. 1000 counts). This is much higher than the background in a diffraction pattern of the NIST Si powder (Supporting Information (SI)), which was collected with the same exposure time and gives a background at ca. 400 counts. Therefore, this enhanced background could be accounted for by the presence of amorphous phase(s) in the "$EuAg_{3.5}Al_{7.5}$" sample, although EDS measurements are consistent with the crystalline phases identified in each pattern shown in Figure 2. A second possible reason for this background originates from the intrinsically disordered distribution

(22) Dronskowski, R.; Blöchl, P. *J. Phys. Chem.* **1993**, *97*, 8617.
(23) Dresse, G.; Joubert, D. *Phys. Rev.* **1999**, *59*, 1758.
(24) Perdew, J. P.; Burke, K.; Ernzerhof, M. *Phys. Rev. Lett.* **1996**, *77*, 3865.
(25) Monkhorst, H. J.; Pack, J. D. *Phys. Rev. B* **1976**, *13*, 5188.
(26) Blöchl, P. E.; Jepsen, O.; Andersen, O. K. *Phys. Rev. B* **1994**, *49*, 16223.

of Ag and Al atoms within each component. At this point, we cannot identify unequivocally the cause of the enhanced background.

Rietveld refinement was then applied to the powder pattern and the results are listed in Tables 1 and 2. Although powder XRD characterizes this sample as a "pure phase", it was very difficult to find a good quality single crystal from this annealed "$EuAg_{3.5}Al_{7.5}$" sample. We extracted only one single crystal which was qualified and carried out single crystal XRD and refinement upon it. The results are also listed in Tables 1 and 2.

Comparison shows that the Rietveld and the single crystal refinements agree well with one another in lattice parameter (with 0.2% difference) and atomic positions. The refined compositions differ slightly from one another: the single crystal technique gives $EuAg_{3.5(2)}Al_{7.5(2)}$, which is very close to the loading composition; but Rietveld refinement gave higher Ag content, $EuAg_{3.67(3)}Al_{7.33(3)}$. Moreover, the isotropic displacement parameters (U_{iso}) refined by the Rietveld technique are much smaller.

Just like many other RE−Ag−Al phases, Ag and Al share the same sites (8*g*, 12*i*, 12*j*) in the asymmetric unit, but these sites are not shared equally. Compared with the average Ag/Al ratio (3.5/7.5 = 0.32/0.68), the 8*g* site prefers Ag and the 12*i* site favors Al. An even higher preference occurs on the 1*b* site, which is exclusively occupied by Ag. We attempted refinement with this site being shared by Ag and Al: it gave the occupancy Ag/Al = 0.94/0.06(7); and the corresponding *R* values are *R*1 = 0.0599 and *wR*2 = 0.0961, which is not a statistically significant improvement over the other refinement, according to a Hamilton test.[27] Therefore, we assigned solely Ag to the 1*b* site. This result agrees with Cordier's study[28] of $BaHg_{11}$-type $CaAg_4Al_7$, in which this site was also filled with only Ag.

The $BaHg_{11}$-type structure has been described in some earlier reports.[28−30] It can be understood by a structure scheme based on a "tetrahedron star", which is a tetrahedron with every face capped by an atom. In a unit cell of $BaHg_{11}$-type $EuAg_{3.5}Al_{7.5}$ (Figure 3(a)), there are eight tetrahedra formed by Ag/Al2(8*g*) and Ag/Al4(12*j*) sites. The Ag1(1*b*) site caps one face of each tetrahedron, which makes Ag1(1*b*) sit in a cuboctahedron formed by Ag/Al4(12*j*) (Figure 3(b)). The Ag/Al3(12*i*) sites cap all of the other faces of the eight tetrahedra. The Eu atom sits in the center of a polyhedron shown in Figure 3(c). The Ag/Al atoms surrounding Eu form five squares. The Eu atom centers a square formed by Ag/Al4(12*j*) atoms, which is "sandwiched" by two larger squares formed by Ag/Al3-(12*i*) atoms and two smaller squares formed by Ag/Al2-(8*g*) atoms. Selected interatomic distances are listed in Table 3. These distances are calculated from lattice parameters from powder data and atomic positions from single crystal data. It shows that the Ag/Al−Ag/Al distances are not uniform in this structure: those involving Ag/Al3(12*i*) (ca. 2.63−2.77 Å) are shorter than the others (>2.87 Å). These distances in the $BaHg_{11}$-type phase are comparable to those observed in $BaCd_{11}$-type $EuAg_xAl_{11-x}$.[9]

Table 1. Summary of Crystal Structure Refinement Parameters of the Annealed "$EuAg_{3.5}Al_{7.5}$" Sample

space group	$Pm\bar{3}m$ (No. 221)	
Z	3	
refinement methods	Rietveld	single crystal
lattice parameters	a = 8.70063(6) Å	a = 8.7208(10) Å
empirical formula	$EuAg_{3.67(3)}Al_{7.33(3)}$	$EuAg_{3.5(2)}Al_{7.5(2)}$
volume	658.645(9) Å^3	663.24(13) Å^3
2θ range	10.00°-90.00°	4.68°-53.26°
goodness-of-fit	1.354	1.178
R indices	R_p = 0.0285	*R*1 = 0.0599 (I > 2σ(I))
	R_{wp} = 0.0374	*wR*2 = 0.0963 (I > 2σ(I))
	R_{exp} = 0.0322	*R*1 = 0.0937 (all data)
	R_B = 0.024	*wR*2 = 0.1039 (all data)
reflections collected		2207
independent reflections		181 (R_{int} = 0.2145)
index ranges		$-9 \le h \le 11$; $-11 \le k \le 8$; $-9 \le l \le 11$
largest diff. peak/hole		1.809/−1.777 e$^-$/ Å^3

Several variants of the $BaHg_{11}$-type structure have been reported for ternary aluminides and indides.[10,31,32] The variances occur in two aspects: the 1*a* (0, 0, 0) site being stuffed with metals, for example, Ag, Au, Pd, or In; and of splitting the 12*i* site. We also introduced these two variances to our refinement of the $BaHg_{11}$-type structure to see whether we could obtain any improvements. Stuffing the 1*a* with Ag gave a negative occupancy on this site. Allowing 12*i* site splitting lowered the *R* values (*R*1 = 0.0578, *wR*2 = 0.0889), but according to a Hamilton test,[27] this change is not a statistically significant improvement. Moreover, the split 12*i* sites are problematic: they have much higher uncertainties in atomic coordinates (see SI Tables S1 and S2). Therefore, our $BaHg_{11}$-type phase does not have these reported structural variances.

EDS and Homogeneity Range. Although powder XRD can detect only the $BaHg_{11}$-type structure in the annealed "$EuAg_{3.5}Al_{7.5}$" sample, its SEM image (Figure 4) reveals that it is not a completely homogeneous phase, which explains why it was difficult to extract good-quality single crystals for XRD. Figure 4 shows a light-gray background (e.g., spots 3, 4, 5, and 6, the major phase) including some patches (the minor phases) in different colors: darker gray (e.g., spots 1 and 2), white (e.g., spot 7), gray with white outline (e.g., spot 8), and black (e.g., spots 9). The compositions on spots 1−9 were analyzed by EDS and are listed in Table 4. The light-gray background is the dominant phase, which is the $BaHg_{11}$-type phase according to powder XRD. The sampling spots (3−6) on the gray background give compositions with small variations but also all are very close to $EuAg_{4.0}Al_{7.0}$, which

(27) Hamilton, W. C. *Acta Crystallogr*. **1965**, *18*, 502.
(28) Cordier, G.; Czech, E.; Schäfer, H. *J. Less-Common Met*. **1985**, *108*, 225.
(29) Häussermann, U.; Svensson, C.; Lidin, S. *J. Am. Chem. Soc*. **1998**, *120*, 3867.
(30) Pearson, W. B. *Z. Kristallogr*. **1980**, *152*, 23.
(31) Gladyshevskii, R. E.; Cenzual, K. *J. Alloys Comp*. **1996**, *240*, 266.
(32) Li, B.; Corbett, J. D. *Inorg. Chem*. **2006**, *45*, 3861.

Table 2. Atomic coordinates and Isotropic Displacement Parameters from Crystal Structure Refinement of the Annealed "$EuAg_{3.5}Al_{7.5}$" Sample

					Rietveld refinement			single crystal refinement		
atom	Wyck.	*x*	*y*	*z*	coordinates	SOF	U_{iso} /Å^2	coordinates	SOF	U_{iso} /Å^2
Eu1	3*d*	1/2	0	0		1	0.0051(3)		1	0.014(1)
Ag1	1*b*	1/2	1/2	1/2		1	0.0065(6)		1	0.030(2)
Ag/Al2	8*g*	*x*	*x*	*x*	$x = 0.1640(1)$	0.416/0.584(4)	0.0146(5)	$x = 0.1658(4)$	0.41/0.59(2)	0.035(2)
Ag/Al3	12*i*	0	*y*	*y*	$y = 0.3453(2)$	0.204/0.796(3)	0.0114(5)	$y = 0.3444(5)$	0.23/0.77(2)	0.023(2)
Ag/Al4	12*j*	1/2	*y*	*y*	$y = 0.2661(1)$	0.353/0.647(2)	0.0060(4)	$y = 0.2667(3)$	0.30/0.70(1)	0.015(2)

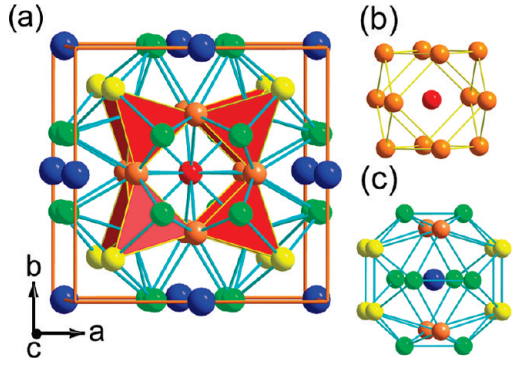

Figure 3. Crystal structures of $BaHg_{11}$-type $EuAg_xAl_{11-x}$: (a) unit cell; (b) the coordination environment of Ag1(1*b*); and (c) the coordination environment of Eu1(3*d*). Blue: Eu1(3*d*); red: Ag1(1*b*); yellow: Ag/Al2(8*g*); green: Ag/Al3(12*i*); orange: Ag/Al4(12*j*).

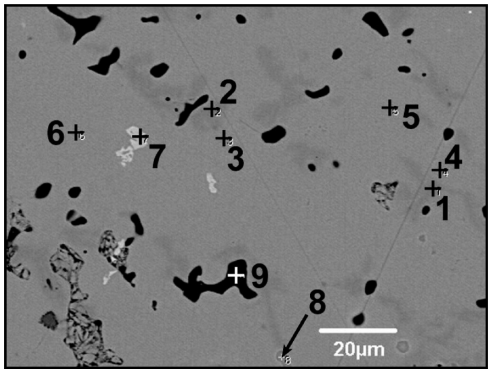

Figure 4. SEM image of the "$EuAg_{3.5}Al_{7.5}$" sample annealed at 500 °C for 40 days. Elemental analysis with EDS was performed on the nine spots marked as 1−9.

Table 3. Selected Interatomic Distances of the $BaHg_{11}$-Type $EuAg_xAl_{11-x}$, Calculated from the Lattice Parameters (Rietveld) and Atomic Positions (Single Crystal) of the Annealed "$EuAg_{3.5}Al_{7.5}$" Sample

atom pair		distances /Å
Eu1−	Ag/Al2 (×8)	3.5521(4)
	Ag/Al3 (×8)	3.288(2)
	Ag/Al4 (×4)	3.281(4)
Ag1−	Ag/Al4 (×12)	2.870(4)
Ag/Al2−	Ag/Al2 (×3)	2.885(8)
	Ag/Al3 (×3)	2.629(5)
Ag/Al3−	Ag/Al3 (×2)	2.708(8)
	Ag/Al4 (×4)	2.771(2)
Ag/Al4−	Ag/Al4 (×4)	2.870(4)

Table 4. EDS Composition Analysis Results of "$EuAg_{3.5}Al_{7.5}$" Annealed at 500 °C for 40 Days (Spots 1−9 are Marked in Figure 4)

	atomic fraction				
spot	Eu	Ag	Al	composition	structure type
1	0.089(1)	0.303(2)	0.608(5)	$Eu_{1.07(2)}Ag_{3.63(3)}Al_{7.30(6)}$	unknown
2	0.087(1)	0.308(2)	0.605(5)	$Eu_{1.05(2)}Ag_{3.69(3)}Al_{7.26(6)}$	
3	0.088(1)	0.329(3)	0.583(5)	$Eu_{1.05(2)}Ag_{3.95(3)}Al_{7.00(6)}$	$BaHg_{11}$
4	0.090(1)	0.322(3)	0.588(5)	$Eu_{1.08(2)}Ag_{3.87(3)}Al_{7.05(6)}$	
5	0.086(1)	0.333(3)	0.581(5)	$Eu_{1.03(2)}Ag_{4.00(3)}Al_{6.97(6)}$	
6	0.086(1)	0.328(3)	0.586(5)	$Eu_{1.03(2)}Ag_{3.93(3)}Al_{7.04(6)}$	
7	0.085(2)	0.443(3)	0.472(5)	$Eu_{1.02(2)}Ag_{5.31(4)}Al_{5.67(6)}$	$BaCd_{11}$
8	0.205(1)	0.132(2)	0.663(6)	$Eu_{1.02(1)}Ag_{0.66(1)}Al_{3.32(3)}$	$BaAl_4$[a]
9	0.001(1)	0.014(1)	0.984(4)	$Ag_{0.014(1)}Al_{0.984(4)}$	*fcc*

[a] EDS shows that there is also some Si (atomic fraction <0.06) present in and only in the $BaAl_4$-type phase. (That Si appears to be an alloying element in the Al foil.)

indicates greater Ag contents than obtained from XRD refinements. This deviation could, again, be attributed to the heterogeneity of the product, which affects the SOF and thus the composition in refinement.

The minor phases do not manifest themselves in powder XRD, but their structures can be deduced by examining their compositions. The composition at spot 7 (the white patch) is $Eu_{1.02(2)}Ag_{5.31(4)}Al_{5.67(6)}$, which falls in the homogeneity range ($EuAg_5Al_6$−$EuAg_6Al_5$) of the $BaCd_{11}$-type phase.[9] The gray patches with white outline (spot 8) have the compositions close to $Eu(Ag,Al)_4$. This is probably a $BaAl_4$-type phase, which occurs frequently in RE−Ag−Al ternary systems.[8] It is noteworthy that a small amount of Si was found in this phase, with its atomic fraction smaller than 0.06. The Si was identified as an impurity of the Al foil. It was detected only in the $BaAl_4$-type phase but not present in any other phases. The black patches (spot 9) are almost pure Al. The identity of the darker gray patches (spots 1 and 2) cannot be determined at this stage. They are probably closely related to the $BaHg_{11}$-type phase because they also have $EuAg_xAl_{11-x}$ compositions but they are slightly richer in Al (ca. $EuAg_{3.7}Al_{7.3}$) than the dominant $BaHg_{11}$-type phase. Further investigations are necessary.

The annealed "$EuAg_3Al_8$" and "$EuAg_4Al_7$" samples were also analyzed with SEM and EDS (SI). The $BaHg_{11}$-type phases in these two samples also give compositions very close to $EuAg_{4.0}Al_{7.0}$, indicating that the $BaHg_{11}$-type $EuAg_xAl_{11-x}$ at 500 °C has a very narrow homogeneity range around $EuAg_{4.0}Al_{7.0}$. Moreover, in the "$EuAg_4Al_7$" sample, the $BaCd_{11}$-type and $BaHg_{11}$-type phases are both abundant. They are clearly different in composition: the former is $EuAg_5Al_6$−$EuAg_6Al_5$ and the latter is $EuAg_{4.0}Al_{7.0}$; that is, they strictly abide to their homogeneity ranges.

As mentioned above, early transition metals facilitate the formation of $BaHg_{11}$-type structure in RE−Au−Al and RE−Ag−Al systems.[10] Our syntheses involved W

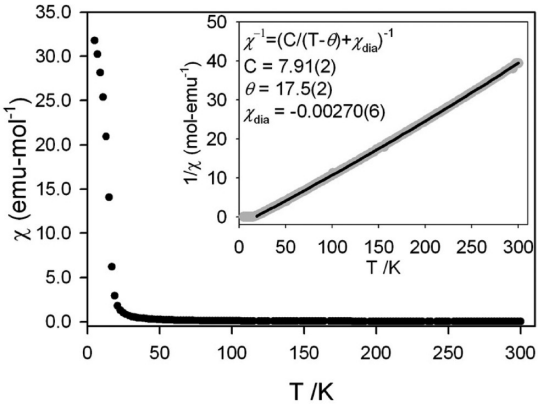

Figure 5. Temperature dependency of magnetic susceptibility and reciprocal susceptibility of the annealed "$EuAg_{3.5}Al_{7.5}$" sample.

(the arc welder electrode), Ti (the oxygen getter for arc melting), and Ta (the container for annealing). However, EDS detected none of these transition metals in the "$EuAg_3Al_8$", "$EuAg_{3.5}Al_{7.5}$", and "$EuAg_4Al_7$" samples. So, under the synthetic conditions we adopted, the formation of $BaHg_{11}$-type $EuAg_xAl_{11-x}$ was not templated by early transition metals.

Thermal Stability. The "$EuAg_{3.5}Al_{7.5}$" sample was subsequently annealed at 600 and 700 °C, each for 10 days, in an attempt to improve its crystallinity and homogeneity. However, the subsequent powder patterns revealed that, at these temperatures, the $BaHg_{11}$-type $EuAg_xAl_{11-x}$ transforms into other phases. After annealing at 600 °C (Figure 2(c)), the $BaHg_{11}$-type phase remained dominant; however, the sample was no longer "pure" because the $BaCd_{11}$-type and Th_2Ni_{17}-type phases emerged. At 700 °C (Figure 2(d)), the $BaHg_{11}$-type phase almost disappeared; and the $BaCd_{11}$-type and Th_2Ni_{17}-type phases became major phases. Therefore, besides composition, the stability of $BaHg_{11}$-type $EuAg_xAl_{11-x}$ is also largely dictated by temperature: at 700 °C, it is no longer thermodynamically stable. This is one of the reasons why $BaHg_{11}$-type RE−Ag−Al phases are less commonly observed than the other phases.

Magnetometry and the Valence Electron Concentration of $BaHg_{11}$-Type $EuAg_xAl_{11-x}$. The temperature dependent magnetic susceptibility (χ) and reciprocal susceptibility ($1/\chi$) of $BaHg_{11}$-type $EuAg_xAl_{11-x}$ is shown in Figure 5. Above 20 K, this phase is paramagnetic and follows the Curie−Weiss law. At ca. 17 K, there is a transition from paramagnetism to ferromagnetism. In the $1/\chi$ vs T curve, the data between 20 and 300 K were fitted with the Curie−Weiss law, from which the effective moment was calculated to be 7.95 μ_B. This value is very close to the μ_{eff} of free Eu^{2+} (7.94 μ_B), indicating the divalency of Eu in this ternary phase.

The valence electron concentration (vec) of $EuAg_xAl_{11-x}$, with respect to the content of electronegative metals Ag and Al, can then be calculated as: $\text{vec} = \frac{2+1\times x+3\times(11-x)}{11} = \frac{35-2x}{11} = 3.18-0.18x$. From this equation, the $BaHg_{11}$-type phases, $EuAg_{4.0}Al_{7.0}$, have a vec at 2.45 e^-/atom. The vec values of some other $BaHg_{11}$-type ternaries are listed in Table 5. All of them

Table 5. Valence Electron Concentration (vec) of Several $BaHg_{11}$-Type Ternary Compounds[a]

compositions	vec	ref.
$EuAg_{4.0}Al_{7.0}$	2.45	
$CaAg_4Al_7$	2.45	28
$YbAg_4Al_7$	2.45	8l
$CeAg_{3.1}Al_{7.9}$	2.71	8k
$YbPd_{2.1-3.4}Ga_{8.9-7.6}$	2.25−2.61	33

[a] The number of valence electrons of Ce, Yb, and Pd are counted as 3, 2, and 0.

are higher than the vec of $BaCd_{11}$-type $REAg_xAl_{11-x}$ (ca. 2.10−2.30 e^-/atom).[9] Therefore, the "rule of thumb" governing the competition between these two 1:11 phases is that the $BaHg_{11}$-type structure is stabilized at higher vec than the $BaCd_{11}$-type structure. The same conclusion was reached by Häussermann[29] in his study of the binary compounds $BaCd_{11}$ and $BaHg_{11}$ with Extended Hückel calculations using second moment scaling. These calculations showed that, although they are isoelectronic (both have vec = 2.18 e^-/atom), the maximum stability of $BaCd_{11}$ occurs at vec = ca. 2.10 e^-/atom, whereas $BaHg_{11}$ is at vec = ca. 2.55 e^-/atom, confirming that vec determines the relative stabilities of these two 1:11 phases. However, this also raises the question for the two binary compounds, $BaCd_{11}$ and $BaHg_{11}$, themselves, namely, why $BaHg_{11}$ does not form the expected $BaCd_{11}$-type structure? Our preliminary study shows that a reason is related to the relativistic effect of the Hg atom, results of which will be discussed in a separate report.

Computational Models. To study how vec affects the stability of the $BaHg_{11}$-type $EuAg_xAl_{11-x}$, it is necessary to analyze its electronic structure through quantum mechanical calculations, for which reasonable model structures need to be built. We constructed the model structures in the following way. The lattice parameters and atomic positions of each model structure were taken from crystallographic data (Table 1 and 2). The 3*d* and 1*b* positions can be unambiguously filled with Eu and Ag. The site sharing between Ag and Al on 8*g*, 12*i*, and 12*j* sites was treated by lowering the symmetry from cubic to triclinic (space group *P*1). The original 8*g* positions were then broken into eight 1*a* positions, which were assigned with 4 Ag and 4 Al atoms (Ag/Al = 0.5/0.5). Likewise, the 12*i* positions were assigned with 3 Ag and 9 Al atoms (Ag/Al = 0.25/0.75) and the 12*j* positions with 4 Ag and 8 Al atoms (Ag/Al = 0.33/0.67). These Ag/Al ratios are very close to those listed in Table 2 and the resulting composition is $EuAg_4Al_7$, which is also close to the experimental value. Then, the "coloring problem"[34] needs to be addressed: fixing the Ag/Al ratios as listed above, there are multiple ($C_8^4 \times C_{12}^3 \times C_{12}^4 = 7\,623\,000$ where $C_n^m = n!/[m! \times (n-m)!]$) possible assignments (or "coloring schemes") of Ag and Al; and we should select the one which gives the lowest total energy. We calculated the total energies with both LMTO and VASP upon several random coloring

(33) Grin, Yu. N.; Hiebl, K.; Rogl, P.; Godart, C.; Alleno, E. *J. Alloys Comp.* **1997**, *252*, 88.
(34) Miller, G. J. *Eur. J. Inorg. Chem.* **1998**, 523.

Table 6. Total Energies of the Model Structures[a]

Model	Coordination Environment of the 3 Eu Atoms (red: Ag; green: Al)	E_{total} per f.u. (eV)		Number of Ag–Al Contacts per Unit Cell	
		LMTO	VASP	< 2.80 Å	< 2.90 Å
1	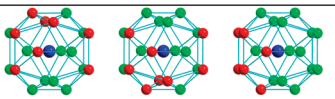	1.38	0.89	30	54
2	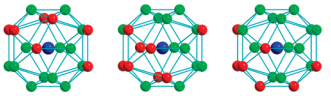	1.00	0.66	36	62
3	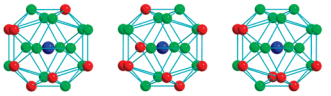	0.58	0.37	40	66
4	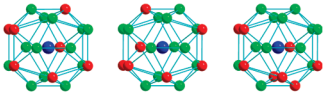	0.33	0.21	44	70
5	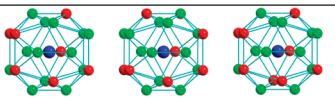	0.00	0.00	50	76

[a] These models all have the same composition ($EuAg_4Al_7$) and same Ag/Al ratio on the original 8*g* (0.5/0.5), 12*i* (0.25/0.75), and 12*j* (0.33/0.67) positions. Models **1**−**4** are random coloring schemes. Model **5** is obtained by maximizing Ag−Al contacts. The total energy of model **5** is taken as reference (0.00 eV). Details of these five models are included in the SI.

schemes (models **1**−**4** in Table 6). Although LMTO gives larger energy differences between coloring schemes than VASP, they show the same trend: the more heteroatomic (Ag−Al) contacts in a coloring scheme, the lower its total energy. The same trend was also discovered in the Ba-Cd_{11}-type $EuAg_xAl_{11-x}$ in our previous study.[9] According to this trend, we constructed model **5** by maximizing Ag−Al contacts (the method of maximizing Ag−Al contacts was described in ref 9). Calculation shows that its total energy is indeed lower than the four random models as expected. Therefore, model **5** is an appropriate model structure for $BaHg_{11}$-type $EuAg_xAl_{11-x}$. The details of models **1**−**5** are included in the SI.

DOS and COHP. The DOS and COHP curves of model **5** calculated with TB-LMTO-ASA are shown in Figure 6. The VASP calculation also gives a DOS curve (SI), which is very close to the one shown in Figure 6. In the DOS curve, the 4*d* bands of Ag manifest as a large peak spanning from ca. −7.5 to ca. −4.5 eV. Leaving this 4*d* peak out, the overall shape of the DOS curve resembles a parabola (the feature of a noninteracting electron gas) with a state-deficient region (pseudogap) at ca. −0.5 to 0.5 eV, corresponding to vec = 2.32−2.58 e^-/atom according to a rigid band approximation. So, when vec = 2.45 e^-/atom ($EuAg_{4.0}Al_{7.0}$), the Fermi level is located in the pseudogap; and the Fermi level falls outside the pseudogap when vec = 2.10−2.30 e^-/atom ($EuAg_5Al_6$−$EuAg_6Al_5$).

The COHP curves for Eu−Ag/Al, Ag−Ag, and Ag−Al contacts have relatively gradual bonding−antibonding crossovers. At vec = 2.45 e^-/atom, the Fermi level is located in their weakly bonding regions. The Al−Al COHP curve, however, has a very steep bonding−antibonding crossover (i.e., Al−Al interactions switch from strongly bonding abruptly to strongly antibonding) and vec = 2.45 e^-/atom locates the Fermi level very close to the crossover (at ca. 2.55 e^-/atom). A vec value much higher than 2.45 e^-/atom will, thus, occupy states that are strongly Al−Al antibonding and destabilize the structure. On the other hand, if the vec is much lower than 2.45 e^-/atom, for example, at 2.10−2.30 e^-/atom, the structure will also be destabilized because those states that are strongly Ag−Ag, Ag−Al, and Al−Al bonding will be largely depleted. Therefore, the vec of 2.45 e^-/atom is

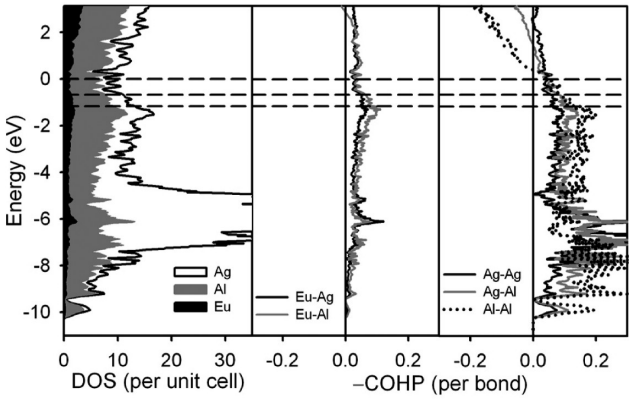

Figure 6. The DOS and COHP curves calculated with model **5** using TB-LMTO-ASA. The three dashed straight line are the locations of the Fermi levels when vec = (from top) 2.45, 2.30, and 2.10 e^-/atom. The parabolic dashed line shows the DOS of the noninteracting electron gas.

very close to the optimum value for the orbital interactions within the Ag/Al framework of the $BaHg_{11}$-type $EuAg_xAl_{11-x}$. By comparison, the vec value that optimizes Ag/Al−Ag/Al interactions in $BaCd_{11}$-type $EuAg_xAl_{11-x}$ is 2.30 e^-/atom.[9] This explains the rule governing the competition between the $BaHg_{11}$- and $BaCd_{11}$-type structures in $EuAg_xAl_{11-x}$ ternary systems: the $BaHg_{11}$-type structure is favored at higher vec (ca. 2.45 e^-/atom) than the $BaCd_{11}$-type structure (ca. 2.30 e^-/atom).

Conclusions

The $BaHg_{11}$-type $EuAg_xAl_{11-x}$ phases were synthesized and characterized. Temperature has important effects on this phase: annealing at 500 °C gives a "pure phase", while it transforms into $BaCd_{11}$- and Th_2Ni_{17}-type phases at 600 and 700 °C. Composition is also pertinent: the cubic $BaHg_{11}$-type structure can only be obtained within a narrow phase around $EuAg_{4.0}Al_{7.0}$, which gives a vec of 2.45 e^-/atom. This value is higher than the vec of the $BaCd_{11}$-type $EuAg_xAl_{11-x}$ phases (2.10−2.30 e^-/atom). First principles electronic structure calculations were performed with a model structure built by simulating crystallographic results and maximizing Ag−Al contacts. The calculation results explained why the $BaHg_{11}$-type structure forms at higher vec value than the $BaCd_{11}$-type structure in the $EuAg_xAl_{11-x}$ system.

Acknowledgment. This work is supported by NSF DMR 02-441092 and 06-05949. We thank Dr. Sumohan Misra and Prof. Vitalij K. Pecharsky for magnetization measurements. We also thank Prof. Susan E. Latturner for her valuable discussions and suggestions.

Supporting Information Available: The results of single crystal refinement with 12*i* site splitting, the SEM and EDS results of the annealed "$EuAg_3Al_8$" and "$EuAg_4Al_7$" samples, the details of models **1**−**5**, the DOS curve of model **5** from VASP calculation, and the powder pattern of the NIST Si powder (PDF). This material is available free of charge via the Internet at http://pubs.acs.org.